Journal of Biomedical Optics

SPIEDigitalLibrary.org/jbo

Whole-body ring-shaped confocal photoacoustic computed tomography of small animals *in vivo*

Jun Xia
Muhammad R. Chatni
Konstantin Maslov
Zijian Guo
Kun Wang
Mark Anastasio
Lihong V. Wang

SPIE

Whole-body ring-shaped confocal photoacoustic computed tomography of small animals *in vivo*

Jun Xia, Muhammad R. Chatni, Konstantin Maslov, Zijian Guo, Kun Wang, Mark Anastasio, and Lihong V. Wang
Washington University in St. Louis, Department of Biomedical Engineering, St. Louis, Missouri 63130

Abstract. We report a novel small-animal whole-body imaging system called ring-shaped confocal photoacoustic computed tomography (RC-PACT). RC-PACT is based on a confocal design of free-space ring-shaped light illumination and 512-element full-ring ultrasonic array signal detection. The free-space light illumination maximizes the light delivery efficiency, and the full-ring signal detection ensures a full two-dimensional view aperture for accurate image reconstruction. Using cylindrically focused array elements, RC-PACT can image a thin cross section with 0.10 to 0.25 mm in-plane resolutions and 1.6 s/frame acquisition time. By translating the mouse along the elevational direction, RC-PACT provides a series of cross-sectional images of the brain, liver, kidneys, and bladder. [DOI: 10.1117/1.JBO.17.5.050506]

Keywords: photoacoustic computed tomography; small-animal imaging; half-time image reconstruction; anatomic imaging.

Paper 12080L received Feb. 6, 2012; revised manuscript received Apr. 4, 2012; accepted for publication Apr. 12, 2012; published online May 4, 2012.

Due to the wide use of animals for human disease studies, small animal whole-body imaging plays an increasingly important role in biomedical research. Currently, the majority of whole-body small-animal anatomic imaging systems are based on magnetic resonance imaging (MRI)[1] or X-ray computed tomography (X-ray CT).[2] However, these imaging techniques have their own limitations, for instance, MRI requires a very high magnetic field and long imaging time (more than 1 h), and X-ray CT utilizes carcinogenic ionizing radiation, which may confound experimental results.[3–5]

Recently, there has been increasing interest in whole-body photoacoustic tomography. Photoacoustic tomography utilizes non-ionizing laser illumination to generate a local temperature rise, which is subsequently converted to pressure via thermoelastic expansion. The pressure waves are detected by ultrasonic transducers, and the temporal signals are reconstructed to form an image of the optical absorbers. The hybrid nature enables photoacoustic tomography to generate high resolution images in both ballistic and diffusive regimes.[6] In the past few years, several whole-body photoacoustic imaging systems, employing different light delivery and acoustic detection schemes, have been proposed.[7–12] However, these systems either have limited detection views, such as half-ring and hemispherical, rendering inaccurate reconstruction of target boundaries,[9,10,12,13] or require long scanning time, which increases motion artifacts.[7,8] The use of fiber bundles also limits the efficiency and uniformity of light delivery. Ideally, a whole-body cross-sectional imaging system should employ uniform free-space ring-shaped light delivery and full-ring ultrasound detection. However, due to the technological difficulties in combining them non-obstructively with animal translation and acoustic coupling mechanisms, this approach has never been demonstrated in photoacoustic whole-body imaging. In this report, we present a ring-shaped confocal photoacoustic computed tomography system (RC-PACT) to overcome the aforementioned limitations and technological difficulties. RC-PACT utilizes free-space full-ring light delivery toward only the image cross section to provide high fluence illumination. The photoacoustic signals are detected by a cylindrically focused 512-element full-ring ultrasonic transducer array. The full-ring coverage enables RC-PACT to provide fast and accurate tomographic inversion of cross-sections with complete boundaries.

Figure 1(a) shows the schematic of RC-PACT. A tunable Ti-Sapphire laser with 12 ns pulse duration and 10 Hz pulse repetition rate was used as the irradiation source. The laser beam was first homogenized using an optical diffuser (EDC-5, RPC Photonics), and then passed through a conical lens (cone angle 130 deg, Delmar Photonics) to form a ring-shaped light. The ring-shaped light was then focused using an optical condenser made from acrylic to project a light band around the animal. The light incident area was aligned to be slightly above the acoustic focal plane to minimize the detection of strong surface signals. The thickness of the light band was 5 mm, and the diameter was determined by the cross-sectional diameter (around 2 cm) of the animal. The maximum light intensity at the surface of the animal was approximately 15 mJ/cm^2, which was below the American National Standards Institute (ANSI) limit at the chosen wavelength.[14]

The photoacoustic signals were detected by a 512-element full-ring transducer array with 5 MHz central frequency (80% bandwidth) and 50 mm ring diameter.[15] Each element in the array was mechanically shaped into an arc to produce an axial focal depth of 19 mm within the imaging plane. The combined foci of all elements generate a central imaging region of 20 mm diameter and 1 mm thickness.[15] This slice thickness and diameter enable tomography for the entire small animal cross section. Within this imaging region, the system provides <0.25 mm tangential (transverse) resolution and relatively uniform 0.10 mm radial (axial) resolution.[15,16] Since the light incidence was oblique, the light formed a weak focus inside the animal body. This focal region overlapped with the acoustic focal plane to improve the efficiency of detecting photoacoustic signals generated in deep tissues. This unique full-ring confocal design enables RC-PACT to have the minimum aperture dimension among existing whole-body photoacoustic tomography systems.[7–12] Our use of free-space ring-shaped light illumination also provides a more uniform light irradiation, and avoids hot spots in images acquired with systems using fiber bundle illumination.[10]

Address all correspondence to: Lihong V. Wang, Washington University in St. Louis, Department of Biomedical Engineering, St. Louis, Missouri 63130; Tel: (314) 935-6152; Fax: (314) 935-7448; E-mail: lhwang@wustl.edu

0091-3286/2012/$25.00

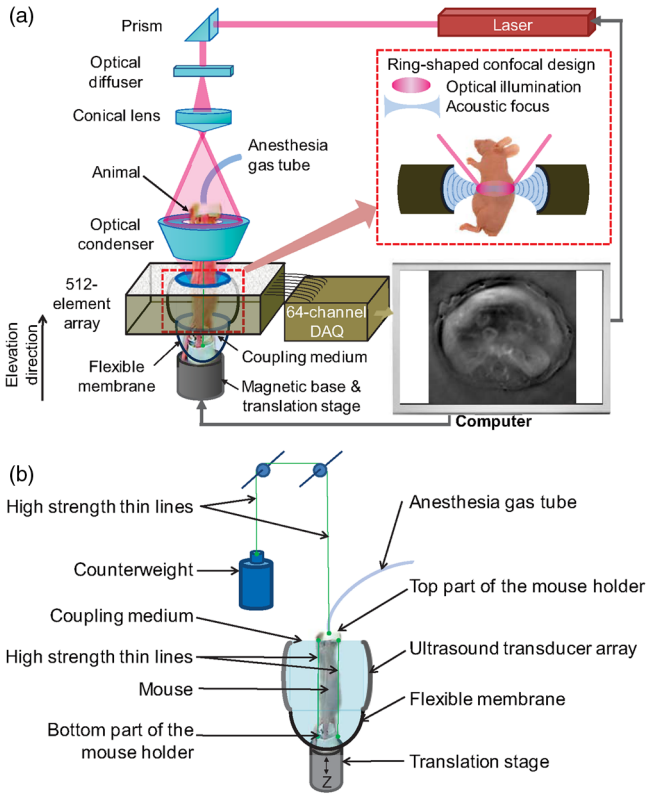

Fig. 1 Experimental setup of the full-ring confocal whole-body photoacoustic computed tomography (RC-PACT) system. (a) Schematic of the RC-PACT system. The dashed box shows a cross-sectional view of the confocal design. (b) A detailed view of the animal holder.

Figure 1(b) is a detailed view of the animal holder, which held the animal upright during imaging. The top part of the holder was a small aluminum tube to fit the animal's nose and mouth, and the bottom part was an aluminum cylinder embedded with a permanent magnet. The magnetic base securely attached the animal holder to the scanning stage underneath the water tank for alignment and three-dimensional scanning. The animal's fore and hind legs were attached to the top and bottom part of the holder using tape. The two parts were connected by high-strength thin lines (0.13 mm diameter braided line). The combination of a magnet and a counterweight put the thin lines in tension to minimize holder movement caused by animal motion. Compared to animal holders using fiberglass rods[8] and plastic tubes[10,17] as the structural elements, the thin lines have negligible light and acoustic blockages, enabling full-ring light delivery and ultrasound detection.

In terms of image reconstruction, the raw data from each element was first Wiener deconvolved to account for the ultrasonic transducer's impulse response and then reconstructed within each imaging plane. The half-time image reconstruction algorithm was used to reconstruct a cross-sectional image of the object to mitigate the artifacts induced by the acoustic heterogeneities in the animal body.[18] The half-time algorithm is based on the principle that the first half of the data propagates through the acoustic heterogeneity over shorter path lengths than the second half, and is less distorted. Because the full data set contains more information than required theoretically for stable image reconstruction, accurate images can still be iteratively restored with the half-time data.[18] On an Intel 2.8 GHz processor, the iterative reconstruction took 20 s per iteration. For experiments acquiring only structural information, a simplified approach using back-projection of the half-time data can be employed. The back-projection image reconstruction took less than 1 s, making the system capable of real-time visualization of the results. Video 1 shows a comparison of reconstructed images using the half-time (right) and the full-time (left) data. It can be seen that the half-time reconstruction renders much clearer images. The arc-shaped streaking artifacts in full-time reconstructed images mainly come from acoustic reflections from the gastrointestinal (GI) tract and spinal cord.

To demonstrate the *in vivo* anatomical imaging capability of our RC-PACT system, we imaged healthy athymic (nude) mice. Figure 2 shows serial cross-sectional images of 5 to 6-week-old healthy athymic mice in axial views.

By mounting the animal underneath the water tank, the system can image the brain through the flexible membrane.[15] Figure 2(a) is an *in vivo* cortical vessel image acquired through the intact scalp and skull. Because the cortical vessels are close to the brain surface (~1 mm), planar top illumination from an optical parametric oscillator laser emitting 532 nm wavelength light was used in the experiment. Alternatively, the animal's head can be kept above the water surface using the aforementioned mounting scheme, which allowed acquisitions of Fig. 2(b)–2(d).

Figure 2(b)–2(c) was acquired at 760 nm and formed purely based on the endogenous hemoglobin contrast. The liver, spleen, and kidneys are clearly visible. Additionally, detailed vascular structures within these organs are visible, demonstrating that the system can be used for static and dynamic[19] whole-body angiographic imaging. The spinal cord, stomach, and GI tracts are

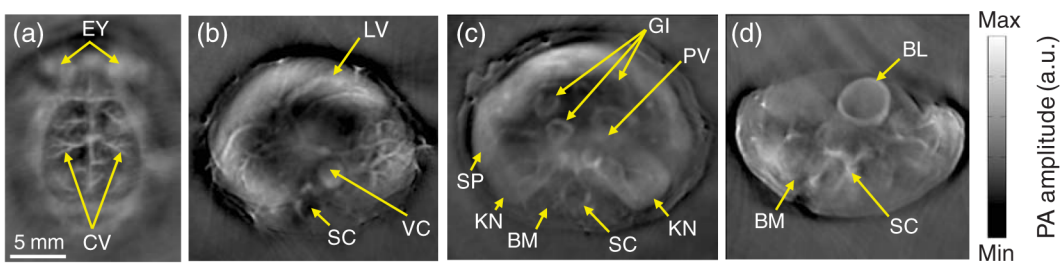

Fig. 2 *In vivo* RC-PACT images of athymic mice acquired noninvasively at various anatomical locations: (a) the brain, (b) the liver (Video 2), (c) the kidneys (Video 1; Video 3), and (d) the bladder (Video 4). Serial images from the heart to the lower abdomen region are available in Video 5. BL, bladder; BM, backbone muscle; CV, cortical vessels; EY, eyes; GI, GI tract; KN, kidney; LV, liver; PV, portal vein; SC, spinal cord; SP, spleen; and VC, vena cava. (Video 1, MOV, QuickTime, 1 KB). [URL: http://dx.doi.org/10.1117/1.JBO.17.5.050506.1]Video 2, MOV, QuickTime, 1 KB [URL: http://dx.doi.org/10.1117/1.JBO.17.5.050506.2]Video 3, MOV, QuickTime, 1.5 KB [URL: http://dx.doi.org/10.1117/1.JBO.17.5.050506.3]Video 4, MOV, QuickTime, 1 KB [URL: http://dx.doi.org/10.1117/1.JBO.17.5.050506.4]Video 5, MOV, QuickTime, 2 KB [URL: http://dx.doi.org/10.1117/1.JBO.17.5.050506.5]

imaged due to the surrounding microvasculature. Major blood vessels, such as the vena cava, are also clearly visible. A series of *in vivo* cross-sectional images acquired around the liver and kidney regions can be found in Videos 2 and 3, respectively. It should be noted that there are some negative-valued pixels in the reconstructed images, which are mainly due to the partial detection view. Using exogenous optical contrast (e.g., near-infrared dyes), the system can also image organs with little blood. Figure 2(d) is an *in vivo* image of a mouse bladder acquired 30 min after tail vein administration of IRDye800, a near-infrared dye. The peak absorption wavelength (776 nm) of the dye was used in the experiment. The urinary bladder showed strong contrast as it was filled with the dye excreted by the kidneys. In Fig. 2(d), the spinal cord and the vessels in the backbone muscles are also clearly shown due to the endogenous hemoglobin contrast. Video 4 shows a series of *in vivo* images acquired over an elevational distance of 6 mm around the bladder.

Each image in Fig. 2 was acquired with 10 times averaging, which took 16 s. The imaging speed of RC-PACT is comparable to CT and faster than MRI, which may take hours for small animal imaging.[20] In principle, RC-PACT can image even faster using a 512-channel data acquisition system, where real-time imaging can be achieved at a frame rate that equals the laser pulse repetition rate.

To showcase the capability of continuous whole-body scanning, we imaged a mouse over a 40 mm range from the heart to the lower abdomen region. The serial *in vivo* images are shown in Video 5. During the scan, in order to minimize the motor-induced motion, the mouse was translated in the elevational direction at a speed of 30 μm/s, and the image acquisition took 25 min, rendering 900 slices. Each image shown in Video 5 was an average of four adjacent slices.

In comparison with existing whole-body photoacoustic tomography systems, the unique design of confocal full-ring light delivery and ultrasound detection in RC-PACT enables fast and accurate tomographic inversion of full-view cross-sectional images. In contrast, the half-ring[10] and the hemispherical[9] based photoacoustic tomography systems have limited detection views and suffer associated image reconstruction artifacts.[12] The photoacoustic tomography system using a rotational arc detector[8] has more coverage of the object; however, it requires 8 min of scanning time, which increases the motion artifacts. Moreover, due to the use of unfocused transducers, the image can only be reconstructed after a complete three-dimensional (3-D) scan, making real-time imaging impossible. RC-PACT's imaging speed of 1 frame per 1.6 s can be further improved by using a 512-channel data acquisition system, where each laser pulse can generate a cross-sectional image nearly free of motion artifacts.

Besides anatomical imaging, RC-PACT can also benefit from the wide choice of optical contrasts, such as near-infrared dyes[21] and fluorescent proteins[22] for functional and molecular imaging. Due to the fixed ring diameter of the current system, we only demonstrated 1 cm penetration depth; however, photoacoustic imaging at depth of 5.2 cm has been reported.[23] Taking advantage of the full-ring light illumination, which doubles the imaging capability to ~10.4 cm diameter, RC-PACT can potentially be scaled to image larger animals. The in-plane and elevational resolutions may be scaled accordingly.

Acknowledgments

The authors appreciate Ms. Seema Dahlheimer's close reading of the manuscript. This work was sponsored in part by National Institutes of Health grants R01 EB000712, R01 EB008085, R01 CA134539, U54 CA136398, R01 EB010049, R01 CA157277, and R01 CA159959. L. W. has financial interests in Microphotoacoustics, Inc. and Endra, Inc., which, however, did not support this work.

References

1. H. Benveniste and S. Blackband, "MR microscopy and high resolution small animal MRI: applications in neuroscience research," *Prog. Neurobiol.* **67**(5), 393–420 (2002).
2. D. W. Holdsworth and M. M. Thornton, "Micro-CT in small animal and specimen imaging," *Trends Biotechnol.* **20**(8), S34–S39 (2002).
3. D. J. Brenner and E. J. Hall, "Computed tomography—an increasing source of radiation exposure," *New Engl. J. Med.* **357**(22), 2277–2284 (2007).
4. R. Fazel et al., "Exposure to low-dose ionizing radiation from medical imaging procedures," *New Engl. J. Med.* **361**(9), 849–857 (2009).
5. G. Brix et al., "Radiation exposure of patients undergoing whole-body dual-modality 18F-FDG PET/CT examinations," *J. Nucl. Med.* **46**(4), 608–613 (2005).
6. L. V. Wang, "Multiscale photoacoustic microscopy and computed tomography," *Nat. Photonics* **3**(9), 503–509 (2009).
7. K. H. Song and L. V. Wang, "Noninvasive photoacoustic imaging of the thoracic cavity and the kidney in small and large animals," *Med. Phys.* **35**(10), 4524–4529 (2008).
8. H.-P. Brecht et al., "Whole-body three-dimensional optoacoustic tomography system for small animals," *J. Biomed. Opt.* **14**(6), 064007–064008 (2009).
9. R. Kruger et al., "HYPR-spectral photoacoustic CT for preclinical imaging," *Proc. SPIE* **7177**, 71770F (2009).
10. A. Buehler et al., "Video rate optoacoustic tomography of mouse kidney perfusion," *Opt. Lett.* **35**(14), 2475–2477 (2010).
11. R. B. Lam et al., "Dynamic optical angiography of mouse anatomy using radial projections," *Proc. SPIE* **7564**, 756405 (2010).
12. D. Razansky, A. Buehler, and V. Ntziachristos, "Volumetric real-time multispectral optoacoustic tomography of biomarkers," *Nat. Protocols* **6**(8), 1121–1129 (2011).
13. Y. Xu et al., "Reconstructions in limited-view thermoacoustic tomography," *Med. Phys.* **31**(4), 724–733 (2004).
14. American National Standards Institute, "American National Standard for the safe use of lasers," American National Standards Institute, New York (2000).
15. J. Gamelin et al., "A real-time photoacoustic tomography system for small animals," *Opt. Express* **17**(13), 10489–10498 (2009).
16. J. Xia et al., "Three-dimensional photoacoustic tomography based on the focal-line concept," *J. Biomed. Opt.* **16**(9), 090505 (2011).
17. D. R. Reinecke et al., "Co-registered photoacoustic, thermoacoustic, and ultrasound mouse imaging," *Proc. SPIE* **7564**, 756420–756429 (2010).
18. M. A. Anastasio et al., "Half-time image reconstruction in thermoacoustic tomography," *IEEE Trans. Med. Imag.* **24**(2), 199–210 (2005).
19. C. Li et al., "Real-time photoacoustic tomography of cortical hemodynamics in small animals," *J. Biomed. Opt.* **15**(1), 010509–010501-010503 (2010).
20. M. Baker, "Whole-animal imaging: the whole picture," *Nature* **463**(7283), 977–980 (2010).
21. L. Meng-Lin et al., "Simultaneous molecular and hypoxia imaging of brain tumors in vivo using spectroscopic photoacoustic tomography," *Proc. IEEE* **96**(3), 481–489 (2008).
22. G. S. Filonov et al., "Deep-tissue photoacoustic tomography of a genetically encoded near-infrared fluorescent probe," *Angew. Chem. Int. Ed.* **51**(6), 1448–1451 (2012).
23. C. Kim et al., "Deeply penetrating in vivo photoacoustic imaging using a clinical ultrasound array system," *Biomed. Opt. Express* **1**(1), 278–284 (2010).